REFERENCES

[1] H. Freeman and L. Garder, "Apictorial jigsaw puzzles: The computer solution of a problem in pattern recognition," *IEEE Trans. Electron. Comput.*, vol. EC-13, pp. 118-127, Apr. 1964.

[2] G. M. Radack and N. I. Badler, "Jigsaw puzzle matching using a boundary-centered polar encoding," *Comput. Graphics Image Processing*, vol. 19, pp. 1-17, 1982.

[3] H. Wolfson, E. Schonberg, A. Kalvin, and Y. Lamdan, "Solving jigsaw puzzles using computer vision," *Ann. Oper. Res.*, vol. 12, pp. 51-64, 1988.

[4] N. Ayache and O. D. Faugeras, "HYPER: A new approach for the recognition and positioning of two-dimensional objects," *IEEE Trans. Pattern Anal. Machine Intell.*, vol. PAMI-8, pp. 44-54, Jan. 1986.

[5] J. L. Turney, T. N. Mudge, and R. A. Volz, "Recognizing partially occluded parts," *IEEE Trans. Pattern Anal. Machine Intell.*, vol. PAMI-7, no. 4, pp. 410-421, July 1985.

[6] A. Kalvin, E. Schonberg, J. T. Schwartz, and M. Sharir, "Two dimensional model based boundary matching using footprints," *Int. J. Robotics Res.*, vol. 5, no. 4, pp. 38-55, 1986.

[7] H. Wolfson, "On curve matching," in *Proc. IEEE Comput. Soc. Workshop Computer Vision*, Miami Beach, FL, Nov. 1987, pp. 307-310.

[8] M. D. Ernst and B. E. Flinchbaugh, "Image/map correspondence using curve matching," presented at the AAAI Robot Navigation Symp., Mar. 28-30, 1989.

[9] J. T. Schwartz and M. Sharir, "Identification of partially obscured objects in two dimensions by matching of noisy characteristic curves," *Int. J. Robotics Res.*, vol. 6, no. 2, pp. 29-44, 1987.

[10] H. Freeman, "Shape description via the use of critical points," *Pattern Recogn.*, vol. 10, pp. 159-166, 1978.

[11] J. Hong and H. J. Wolfson, "An improved model-based matching method using footprints," in *Proc. Int. Conf. Pattern Recognition*, Rome, Italy, Nov. 1988, pp. 72-78.

[12] P. Weiner, "Linear pattern matching algorithms," in *Proc. 14th Annu. Symp. Switching and Automata Theory*, IEEE Comput. Soc., 1973, pp. 1-11.

[13] M. McCreight, "A space-economical suffix tree construction algorithm," *J. ACM*, vol. 23, no. 2, pp. 262-272, Apr. 1976.

[14] D. T. Lee and F. P. Preparata, "Euclidean shortest paths in the presence of rectilinear bariers," *Networks*, vol. 14, pp. 393-410, 1984.

[15] J. J. Stoker, *Differential Geometry*. New York: Wiley-Interscience, 1969.

[16] E. Kishon and H. Wolfson, "3-D curve matching," in *Proc. AAAI Workshop Spatial Reasoning and Multisensor Fusion*, St. Charles, IL, Oct. 1987, pp. 250-261.

Invariant Image Recognition by Zernike Moments

ALIREZA KHOTANZAD AND YAW HUA HONG

***Abstract*—This correspondence addresses the problem of rotation, scale, and translation invariant recognition of images. A new set of rotation invariant features are introduced. They are the magnitudes of a set of orthogonal complex moments of the image known as Zernike moments. Scale and translation invariance are obtained by first normalizing the image with respect to these parameters using its regular geometrical moments. A systematic reconstruction-based method for deciding the highest order of Zernike moments required in a classification problem is developed. The "quality" of the reconstructed image is examined through its comparison to the original one. More moments are included until the reconstructed image from them is close enough to the original picture. The orthogonality property of the Zernike moments which simplifies the process of image reconstruction makes the suggested feature selection approach practical. Furthermore, features of each order can also be weighted according to their contribution (their image representation ability) to the reconstruction process. The method is tested using clean and noisy images from a 26-class character data set and a 4-class lake data set. The superiority of Zernike moment features over regular moments and moment invariants is experimentally verified.**

***Index Terms*—Feature selection, image recognition, image reconstruction, invariant pattern recognition, moment invariants, Zernike moments.**

Manuscript received August 29, 1988; revised October 13, 1989. Recommended for acceptance by C. Y. Suen. This work was supported in part by the Defense Advanced Research Projects Agency under Grant MDA-903-86-C-0182.

A. Khotanzad is with the Image Processing and Analysis Laboratory, Department of Electrical Engineering, Southern Methodist University, Dallas, TX 75275.

Y. H. Hong was with the Image Processing and Analysis Laboratory, Department of Electrical Engineering, Southern Methodist University, Dallas, TX 75275. He is now with Texas Instruments Incorporated, Dallas, TX.

IEEE Log Number 8933763.

I. INTRODUCTION

An important problem in pattern analysis is the automatic recognition of an object in a scene regardless of its position, size, and orientation. They arise in a variety of situations such as inspection and packaging of manufactured parts [14], classification of chromosomes [3], target identification [2], [15], and scene analysis [5]. The current approaches to invariant two-dimensional shape recognition include extraction of global image information using regular moments [15], boundary-based analysis via Fourier descriptors [12], [14], [15], [18], or autoregressive models [9], image representation by circular harmonic expansion [6], and syntactic approaches [3]. A fundamental element of all these schemes is definition of a set of features for image representation and data reduction. Normally additional transformations are needed to achieve the desired invariant properties for the selected features. After invariant features are computed, they are input to a designed classification rule to decide a labeling for the underlying image. The utilization of good features is not the only decisive factor in the success of these methods. An additional parameter to be decided upon is the number of such features to be used. However, the majority of the existing techniques use an ad hoc procedure for arriving at such a decision. The aim of this work is to develop new features along with a systematic method for selection of the required number of features needed.

Moments and functions of moments have been utilized as pattern features in a number of applications [1], [2], [7], [15]. Such features capture global information about the image and do not require closed boundaries as boundary-based methods such as Fourier descriptors do. Regular moments have by far been the most popular type of moments. They are defined as

$$m_{pq} = \int_{-\infty}^{\infty} \int_{-\infty}^{\infty} x^p y^q f(x, y)\, dx\, dy \tag{1}$$

where m_{pq} is the $(p + q)$th order moment of the continuous image function $f(x, y)$. For digital images the integrals are replaced by summations and m_{pq} becomes

$$m_{pq} = \sum_x \sum_y x^p y^q f(x, y). \tag{2}$$

Hu [7] introduced seven nonlinear functions defined on regular moments which are translation, scale, and rotation invariant. These

seven so called moment invariants were used in a number of pattern recognition problems [2], [13].

The definition of regular moments has the form of projection of $f(x, y)$ function onto the monomial $x^p y^q$. Unfortunately, the basis set $x^p y^q$ is not orthogonal. Consequently, the recovery of image from these moments is quite difficult and computationally expensive. Moreover, it implies that the information content of m_{pq}'s have a certain degree of redundancy. Teague [16] has suggested the orthogonal moments based on the theory of orthogonal polynomials to overcome the problems associated with the regular moments. Zernike moments used in this study are a class of such orthogonal moments. The reason for selecting them from among the other orthogonal moments is that they possess a useful rotation invariance property. Rotating the image does not change the magnitudes of its Zernike moments. Hence, they could be used as rotation invariant features for image representation. These features could easily be constructed to an arbitrary high order. Another main property of Zernike moments is the ease of image reconstruction from them. The orthogonality property enables one to separate out the individual contribution of each order moment (its information content) to the reconstruction process. Simple addition of these individual contributions generates the reconstructed image. Taking advantage of this characteristic, a method for selection of the required number of features (maximum order of moments) is developed. This technique evaluates the image representation ability of features of each order moments through comparison of the reconstructed image by them with the original one. The maximum order required is the one for which the reconstructed image is close to the original one. Furthermore, one can weight the features according to their relative contribution to the reconstruction process.

The defined features on the Zernike moments are only rotation invariant. To obtain scale and translation invariance, the image is first subjected to a normalization process using its regular moments. The rotation invariant Zernike features are then extracted from the scale and translation normalized image.

Teh and Chin [17] examined noise sensitivity and information redundancy of Zernike moments along with five other moments. They concluded that higher order moments are more sensitive to noise. It was also shown that orthogonal moments including Zernike moments are better than other types of moments in terms of information redundancy and image representation.

The organization of this correspondence is as follows. Section II defines the Zernike moments and their properties. In Section III, the image reconstruction from its Zernike moments is shown. Section IV discusses the rotation invariant features obtained from Zernike moments. Section V describes the synthesis based feature selection method. Section VI contains the scale and translation normalization approach and examines the performance of the proposed features and the accompanying feature selection method through experimental studies involving a 26-class English character data set and a 4-class lake data set. Performance comparisons to moment invariants and regular moments are also presented in this section. Section VII gives the conclusion of our study.

II. Zernike Moments

In [19], Zernike introduced a set of complex polynomials which form a complete orthogonal set over the interior of the unit circle, i.e., $x^2 + y^2 = 1$. Let the set of these polynomials be denoted by $\{V_{nm}(x, y)\}$. The form of these polynomials is:

$$V_{nm}(x, y) = V_{nm}(\rho, \theta) = R_{nm}(\rho) \exp(jm\theta) \tag{3}$$

where

- n Positive integer or zero.
- m Positive and negative integers subject to constraints $n - |m|$ even, $|m| \le n$.
- ρ Length of vector from origin to (x, y) pixel.
- θ Angle between vector ρ and x axis in counterclockwise direction.

$R_{nm}(\rho)$ Radial polynomial defined as

$$R_{nm}(\rho) = \sum_{s=0}^{(n-|m|)/2} (-1)^s \cdot \frac{(n-s)!}{s!\left(\frac{n+|m|}{2} - s\right)!\left(\frac{n-|m|}{2} - s\right)!} \rho^{n-2s}.$$

Note that $R_{n,-m}(\rho) = R_{nm}(\rho)$.

These polynomials are orthogonal and satisfy

$$\int\int_{x^2+y^2\le 1} [V_{nm}(x, y)]^* V_{pq}(x, y)\, dx\, dy = \frac{\pi}{n+1} \delta_{np} \delta_{mq}$$

with

$$\delta_{ab} = \begin{cases} 1 & a = b \\ 0 & \text{otherwise.} \end{cases}$$

Zernike moments are the projection of the image function onto these orthogonal basis functions. The Zernike moment of order n with repetition m for a continuous image function $f(x, y)$ that vanishes outside the unit circle is

$$A_{nm} = \frac{n+1}{\pi} \int\int_{x^2+y^2\le 1} f(x, y)\, V^*_{nm}(\rho, \theta)\, dx\, dy. \tag{4}$$

For a digital image, the integrals are replaced by summations to get

$$A_{nm} = \frac{n+1}{\pi} \sum_x \sum_y f(x, y)\, V^*_{nm}(\rho, \theta), \quad x^2 + y^2 \le 1. \tag{5}$$

To compute the Zernike moments of a given image, the center of the image is taken as the origin and pixel coordinates are mapped to the range of unit circle, i.e., $x^2 + y^2 \le 1$. Those pixels falling outside the unit circle are not used in the computation. Also note that $A^*_{nm} = A_{n,-m}$.

III. Image Reconstruction from Zernike Moments

Suppose that one knows all moments A_{nm} of $f(x, y)$ up to a given order $n_{\max}$. It is desired to reconstruct a discrete function $\hat{f}(x, y)$ whose moments exactly match those of $f(x, y)$ up to the given order $n_{\max}$. Zernike moments are the coefficients of the image expansion into orthogonal Zernike polynomials. By orthogonality of the Zernike basis

$$\hat{f}(x, y) = \sum_{n=0}^{n_{\max}} \sum_m A_{nm} V_{nm}(\rho, \theta) \tag{6}$$

with m having similar constraints as in (3). Note that as $n_{\max}$ approaches infinity $\hat{f}(x, y)$ will approach $f(x, y)$.

Since it is easier to work with real-valued functions, one can expand (6) noting that $V^*_{nm}(\rho, \theta) = V_{n,-m}(\rho, \theta)$

$$\begin{aligned}
\hat{f}(x, y) &= \sum_n \sum_{m<0} A_{nm} V_{nm}(\rho, \theta) + \sum_n \sum_{m\ge 0} A_{nm} V_{nm}(\rho, \theta) \\
&= \sum_n \sum_{m>0} A_{n,-m} V_{n,-m}(\rho, \theta) + \sum_n \sum_{m\ge 0} A_{nm} V_{nm}(\rho, \theta) \\
&= \sum_n \sum_{m>0} A^*_{nm} V^*_{nm}(\rho, \theta) + \sum_n \sum_{m\ge 0} A_{nm} V_{nm}(\rho, \theta) \\
&= \left[\sum_n \sum_{m>0} \left[A^*_{nm} V^*_{nm}(\rho, \theta) + A_{nm} V_{nm}(\rho, \theta)\right]\right] \\
&\quad + A_{n0} V_{n0}(\rho, \theta) \\
&= \left[\sum_n \sum_{m>0} \left\{\left[\mathrm{Re}\,[A_{nm}] - j\,\mathrm{Im}\,[A_{nm}]\right] R_{nm}(\rho) \right.\right. \\
&\quad \cdot [\cos m\theta - j \sin m\theta] \\
&\quad + \left[\mathrm{Re}\,[A_{nm}] + j\,\mathrm{Im}\,[A_{nm}]\right] R_{nm}(\rho) \\
&\quad \left.\left. \cdot [\cos m\theta + j \sin m\theta]\right\}\right] \\
&\quad + \left[\mathrm{Re}\,[A_{n0}] + j\,\mathrm{Im}\,[A_{n0}]\right] R_{n0}(\rho)
\end{aligned}$$

$$\hat{f}(x, y) = \sum_{n} \sum_{m>0} (C_{nm} \cos m\theta + S_{nm} \sin m\theta) R_{nm}(\rho) + \frac{C_{n0}}{2} R_{n0}(\rho) \quad (7)$$

with

$$C_{nm} = 2 \operatorname{Re}(A_{nm}) = \frac{2n+2}{\pi} \int\int_{x^2+y^2 \le 1} f(x, y) \cdot R_{nm}(\rho) \cos m\theta \, dx \, dy$$

$$S_{nm} = -2 \operatorname{Im}(A_{nm}) = \frac{-2n-2}{\pi} \int\int_{x^2+y^2 \le 1} f(x, y) \cdot R_{nm}(\rho) \sin m\theta \, dx \, dy.$$

Indeed, C_{nm} and S_{nm} expressions could be used in place of (4) to compute A_{nm} as well.

This reconstruction process is illustrated in Fig. 1 for two 64 × 64 binary images of letters E and F. The reconstructed binary images are generated by using (7) followed by mapping to [0, 255] range, histogram equalization [5], and binarization using threshold of 128. It is evident that lower order moments capture gross shape information and high frequency details are filled in by higher order moments. In this example moments of order 2 through 12 are used. The reason for omitting orders 0 and 1 is due to the nature of preprocessing done on the original images which will be discussed later.

IV. Rotation Invariant Features Derived from Zernike Moments

Consider a rotation of the image through angle α. If the rotated image is denoted by f^r, the relationship between the original and rotated images in the same polar coordinates is

$$f^r(\rho, \theta) = f(\rho, \theta - \alpha). \quad (8)$$

The Zernike moment expression can be mapped from the xy-plane into the polar coordinates by changing the variables in double integral form of (4). This can be seen from [8]

$$\int_A \int \phi(x, y) \, dx \, dy = \int_G \int \phi[p(\rho, \theta), q(\rho, \theta)] \frac{\partial(x, y)}{\partial(\rho, \theta)} \, d\rho \, d\theta \quad (9)$$

where $\partial(x, y)/\partial(\rho, \theta)$ denotes the Jacobian of the transformation and is the determinant of the matrix

$$\frac{\partial(x, y)}{\partial(\rho, \theta)} = \begin{bmatrix} \frac{\partial x}{\partial \rho} & \frac{\partial x}{\partial \theta} \\ \frac{\partial y}{\partial \rho} & \frac{\partial y}{\partial \theta} \end{bmatrix}. \quad (10)$$

For this case where $x = \rho \cos \theta$ and $y = \rho \sin \theta$, the Jacobian becomes ρ. Hence

$$A_{nm} = \frac{n+1}{\pi} \int_0^{2\pi} \int_0^1 f(\rho, \theta) V_{nm}^*(\rho, \theta) \rho \, d\rho \, d\theta = \frac{n+1}{\pi} \int_0^{2\pi} \int_0^1 f(\rho, \theta) R_{nm}(\rho) \exp(-jm\theta) \rho \, d\rho \, d\theta. \quad (11)$$

The Zernike moment of the rotated image in the same coordinate is

$$A_{nm}^r = \frac{n+1}{\pi} \int_0^{2\pi} \int_0^1 f(\rho, \theta - \alpha) R_{nm}(\rho) \exp(-jm\theta) \rho \, d\rho \, d\theta. \quad (12)$$

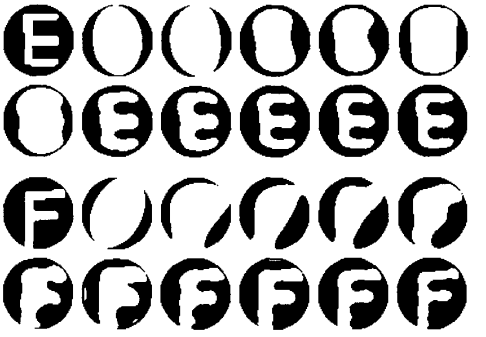

Fig. 1. The reconstructed images of characters E and F. From top row and left to right: original image, reconstructed image with up to second order moment through up to twelfth order moment.

By a change of variable $\theta_1 = \theta - \alpha$

$$A_{nm}^r = \frac{n+1}{\pi} \int_0^{2\pi} \int_0^1 f(\rho, \theta_1) R_{nm}(\rho) \exp(-jm(\theta_1 + \alpha)) \cdot \rho \, d\rho \, d\theta_1 = \left[\frac{n+1}{\pi} \int_0^{2\pi} \int_0^1 f(\rho, \theta_1) R_{nm}(\rho) \cdot \exp(-jm\theta_1) \rho \, d\rho \, d\theta_1 \right] \exp(-jm\alpha) = A_{nm} \exp(-jm\alpha). \quad (13)$$

Equation (13) shows that Zernike moments have simple rotational transformation properties; each Zernike moment merely acquires a phase shift on rotation. This simple property leads to the conclusion that the magnitudes of the Zernike moments of a rotated image function remain identical to those before rotation. Thus $|A_{nm}|$, the magnitude of the Zernike moment, can be taken as a rotation invariant feature of the underlying image function. Note that since $A_{n,-m} = A_{nm}^*$, then $|A_{nm}| = |A_{n,-m}|$; thus, one can concentrate on $|A_{nm}|$ with $m \ge 0$ as far as the defined Zernike features are concerned. Table I lists the rotation invariant Zernike features and their corresponding numbers from order 0 to order 12.

This rotation invariancy property is illustrated by an experiment. Fig. 2 shows a 64 × 64 binary image of character A and five rotated versions of it, with rotation angles of 30°, 60°, 150°, 180°, and 300°, respectively. Table II is the list of the magnitudes of their Zernike moments for orders 2 and 3, their respective sample mean μ, sample standard deviation σ, and $\sigma/\mu\%$, which indicates the percentage of spread of the $|A_{nm}|$ values from their corresponding means. It is observed that rotation invariancy is very well achieved. For example, $\sigma/\mu\%$ is 0.30% and 0.90% for $|A_{20}|$ and $|A_{33}|$, respectively. These are to be compared to the exact invariances of 0%. The reason for not obtaining exact invariances is the discrete form of the image function rather than being a continuous one.

V. Feature Selection Via Reconstruction

Having shown that the magnitudes of Zernike moments can be taken as rotation invariant features, a main question to be answered is; how big should n be? In other words, up to what order moments are needed for a good classification of a given database. In fact, a major shortcoming of many previously developed feature sets for image representation is the lack of a systematic method for automatic selection of this number.

A good set of features is one that can characterize and represent the image well. The difference between an image and its reconstructed version from a finite set of its moments is a good measure

TABLE I
LIST OF ZERNIKE MOMENTS AND THEIR CORRESPONDING NUMBER OF FEATURES FROM ORDER ZERO TO ORDER TWELVE

Order	Moments	No. of Moments
0	A_{00}	1
1	A_{11}	1
2	A_{20}, A_{22}	2
3	A_{31}, A_{33}	2
4	A_{40}, A_{42}, A_{44}	3
5	A_{51}, A_{53}, A_{55}	3
6	A_{60}, A_{62}, A_{64} A_{66}	4
7	A_{71}, A_{73}, A_{75} A_{77}	4
8	A_{80}, A_{82}, A_{84} A_{86}, A_{88}	5
9	A_{91}, A_{93}, A_{95} A_{97}, A_{99}	5
10	$A_{10,0}$, $A_{10,2}$, $A_{10,4}$ $A_{10,6}$, $A_{10,8}$, $A_{10,10}$	6
11	$A_{11,1}$, $A_{11,3}$, $A_{11,5}$ $A_{11,7}$, $A_{11,9}$, $A_{11,11}$	6
12	$A_{12,0}$, $A_{12,2}$, $A_{12,4}$ $A_{12,6}$, $A_{12,8}$, $A_{12,10}$ $A_{12,12}$	7

Fig. 2. The image of character A and five rotated versions of it. From left to right rotation angles are: 0°, 30°, 60°, 150°, 180°, and 300°.

TABLE II
MAGNITUDES OF SOME OF THE ZERNIKE MOMENTS FOR ROTATED IMAGES SHOWN IN FIG. 2 AND THEIR CORRESPONDING STATISTICS

	$\lvert A_{20}\rvert$	$\lvert A_{22}\rvert$	$\lvert A_{31}\rvert$	$\lvert A_{33}\rvert$
0°	439.62	41.79	57.97	172.57
30°	436.70	40.20	63.82	171.96
60°	440.63	40.08	66.28	169.41
150°	438.53	41.55	65.47	170.83
180°	439.01	46.85	62.39	168.47
300°	438.43	39.19	65.77	170.84
μ	438.82	41.61	63.62	170.68
σ	1.32	2.74	3.12	1.53
σ/μ%	0.30	6.57	4.90	0.90

of the image representation ability of the considered set of moments. The ease of image reconstruction from Zernike moments makes it practical to base the feature selection process on such a measure. The idea is that n^*, the maximum needed order, is one which can generate a reconstructed image which is similar to the original in the sense of a defined threshold. In the following discussion, we will concentrate on binary images. However, extension to gray level images is straightforward.

Let $\hat{f}_i$ denote the binary image reconstructed by using moments of order 0 through i extracted from the original image, f. $\hat{f}_i$ is generated using

$$\hat{f}_i(x, y) = F\left(\left|\sum_{n=0}^{i}\sum_{m} A_{nm}V_{nm}(\rho, \theta)\right|\right) \forall\, x, y \qquad (14)$$

where F represents mapping to [0, 255] gray level range, histogram equalization, and thresholding at 128. A simple measure of image representation ability is the difference between $\hat{f}_i$ and the original binary image f. The Hamming distance between the two, $H(\hat{f}_i, f)$ is employed to quantify this difference. The Hamming distance is the total number of pixels that are different in the two images. If $H(\hat{f}_i, f) \le \epsilon$, where ϵ is a preselected threshold, then it can be concluded that enough information is extracted and no additional order of moments needs to be computed, i.e., $n^* = i$.

The above procedure not only specifies the highest order needed for a prototype, but also provides a means for treating features of each order differently. It is apparent that different order moments capture different characteristics of the image. One can isolate the contribution of ith order moments to the reconstruction process and use its relative strength to weight the corresponding features. The contribution of ith order moments to the reconstruction process can be measured by computing how much closer $\hat{f}_i$ is to f compared to $\hat{f}_{i-1}$. Hamming distance is again employed to carry out this task. The contribution of the ith order moments denoted by $C(i)$, is computed as

$$C(i) = H(\hat{f}_{i-1}, f) - H(\hat{f}_i, f). \qquad (15)$$

A large positive value of $C(i)$ indicates that the ith order moments do capture a lot of important information about the shape. On the other hand, a small positive or a negative $C(i)$ is an indication that the corresponding moments focus on unimportant aspects of the image under study. Consequently, it makes sense to weight important (in the sense of reconstruction) moments and their corresponding features more and vice versa. Thus, one can introduce a weighting mechanism for the ith order features based on their corresponding $C(i)$'s. All ith order features could be weighted by w_i during classification stage where,

$$w_i = \frac{C(i)}{D(n^*)} \qquad i = 1, 2, \cdots, n^*, \qquad (16)$$

and

$$D(n^*) = \sum_{j=1, C(j)\ge 0}^{n^*} C(j).$$

If $C(i)$ is negative, w_i is set to zero. Note that the w_i's sum up to 1.0. Fig. 3 and Table III show the synthesized images and the corresponding $C(i)$ and w_i values for character "A" when $\epsilon = 300$ pixels. Again note that the zeroth order and first order moments are not used due to the preprocessing explained later. The weight for the second order moment is set to zero since there is no previous image (i.e., $\hat{f}_1$) for comparison. Also, note that the unit circle part of a 64 × 64 image which consists of 3096 pixels is the basis for comparison and Hamming distance calculation. If more than one prototype exists for a class, each one may give rise to a different n^* and w_i. In that case, the highest n^* and the average of w_i are used.

The same procedure can be used in the case of gray level images. The only needed modification is changing the difference measure from the Hamming distance to either a correlation type measure or mean squared error.

Up to now, the discussion has centered on how to select the right order of moments and feature weights for a single class from its given training samples. In a multiclass problem, the highest order moment to be extracted from an unknown image is $n^*_{\max}$ where $n^*_{\max}$ is the maximum value among all the classes to be considered.

VI. EXPERIMENTAL STUDY

In this section, the classification power of the proposed Zernike moment features and the accompanying feature selection method is experimentally tested and the results are reported. Furthermore, the performance of these features is compared to those of moment invariants and regular moments. Noise sensitivity of Zernike features is also examined.

A. The Utilized Data Sets

Two different data sets of shapes are generated. The first data set consists of 26 upper case English characters from "A" to "Z". Twelve different 64 × 64 binary images from each character (for a total of 314 images) are considered. Four slightly different silhouettes of each character are generated and three scaled, rotated,

Fig. 3. The reconstructed images of character A. From left to right: original image and reconstructed images with up to second order moment through up to seventh order moment. $n^* = 7$ is selected with $\epsilon = 300$.

TABLE III
STATISTICS FOR RECONSTRUCTED IMAGES SHOWN IN FIG. 3

Order i	$H(\mathbf{f}_i, \mathbf{f})$	$C(i)$	w_i
2	908	N/A	0
3	1126	-218	0
4	535	591	.6328
5	492	43	.0460
6	525	-33	0
7	225	300	.3212

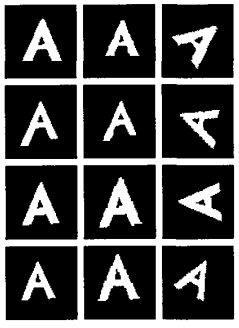

Fig. 4. The twelve scaled, translated, and rotated images of letter A in the character data set. Note the slight intraclass variations in shape.

and translated versions of each silhouette are considered to make up the twelve images per class. Fig. 4 shows the twelve generated images of character "A". Note the within class differences of shapes and their scale, orientation, and translation. In Fig. 5 four (unrotated) out of twelve images of each of the other characters are shown.

The second data set consists of four classes of shapes which are the aerial views of lakes Erie, Huron, Michigan, and Superior. Again twelve differently oriented 64 × 64 binary images of each lake are generated. Fig. 6 shows these images. Note that no within class shape difference is considered for this data set.

As discussed before, the proposed Zernike features are only rotation invariant. But, the considered images have scale and translation differences as well. Therefore, prior to extraction of Zernike features, these images should be normalized with respect to scaling and translation. A regular moment-based approach is taken toward this stage which is discussed in the next section.

B. Scale and Translation Normalization

To achieve scale and translation uniformity, the regular moments (i.e., m_{pq}) of each image are utilized. Translation invariancy is achieved by transforming the image into a new one whose first order moments, m_{01} and m_{10}, are both equal to zero. This is done by transforming the original $f(x, y)$ image into another one which is $f(x + \bar{x}, y + \bar{y})$, where $\bar{x}$ and $\bar{y}$ are the centroid location of the original image computed from

$$\bar{x} = \frac{m_{10}}{m_{00}}, \qquad \bar{y} = \frac{m_{01}}{m_{00}}.$$

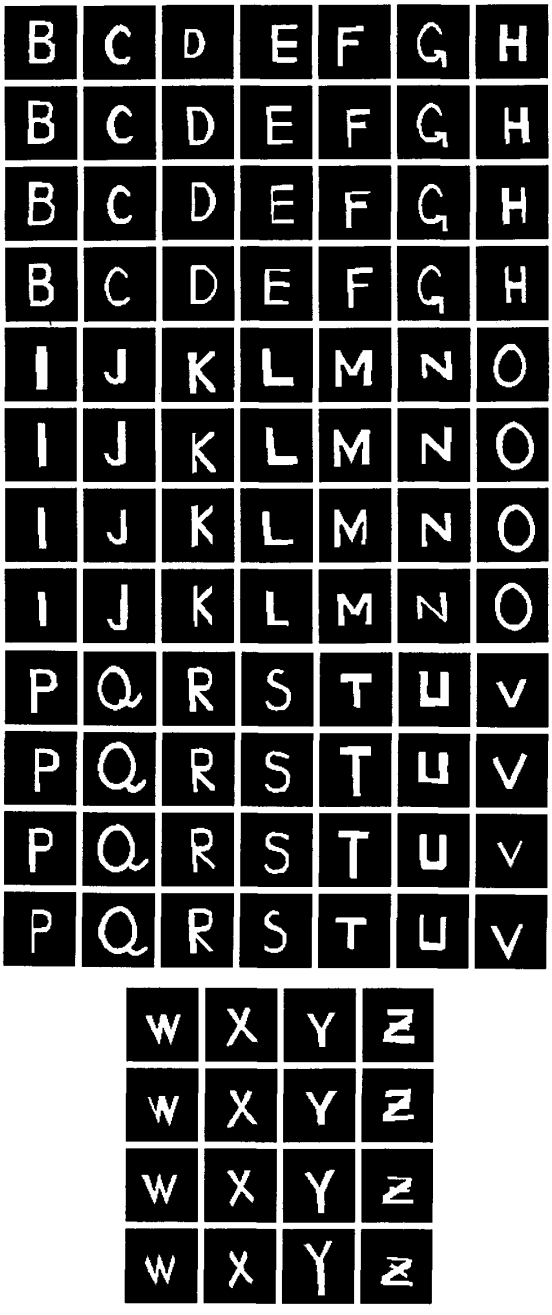

Fig. 5. Four out of the twelve images of letters B to Z in the character data set. The remaining eight images per character are rotated, scaled, and translated versions of the shown four.

In other words, the origin is moved to the centroid before moment calculation.

Scale invariancy is accomplished by enlarging or reducing each shape such that its zeroth order moment m_{00} is set equal to a predetermined value β. Note that in the case of binary images m_{00} is the total number of shape pixels in the image. Let $f(x/a, y/a)$ represent a scaled version of the image function $f(x, y)$. Then, the regular moment m_{pq} of $f(x, y)$ and m'_{pq}, the regular moment of

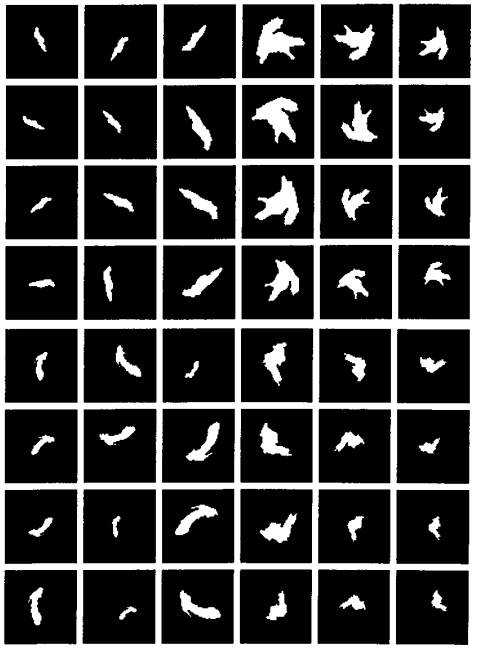

Fig. 6. The twelve scaled, translated, and rotated images of Lakes Erie, Huron, Michigan, and Superior.

$f(x/a, y/a)$, are related by

$$\begin{aligned} m'_{pq} &= \int_x \int_y x^p y^q f\left(\frac{x}{a}, \frac{y}{a}\right) dx\, dy \\ &= \int_x \int_y a^p x^p a^q y^q f(x, y) a^2\, dx\, dy \\ &= \int_x \int_y a^{p+q+2} x^p y^q f(x, y)\, dx\, dy \\ &= a^{p+q+2} \int_x \int_y x^p y^q f(x, y)\, dx\, dy \\ &= a^{p+q+2} m_{pq}. \end{aligned} \tag{17}$$

Since the objective is to have $m'_{00} = \beta$, one can let $a = \sqrt{\beta/m_{00}}$. Substituting $a = \sqrt{\beta/m_{00}}$ into m'_{00}, one obtains $m'_{00} = a^2 m_{00} = \beta$. Thus scale invariancy is achieved by transforming the original image function $f(x, y)$ into a new function $f(x/a, y/a)$, with $a = \sqrt{\beta/m_{00}}$.

In summary, an image function $f(x, y)$ can be normalized with respect to scale and translation by transforming it into $g(x, y)$, where

$$g(x, y) = f\left(\frac{x}{a} + \bar{x}, \frac{y}{a} + \bar{y}\right), \tag{18}$$

with $(\bar{x}, \bar{y})$ being the centroid of $f(x, y)$ and $a = \sqrt{\beta/m_{00}}$, with β a predetermined value. Wherever $(x/a + \bar{x}, y/a + \bar{y})$ does not correspond to a grid location, the function value associated with it is interpolated from the values of the four nearest grid locations around it.

Fig. 7 shows the effect of this normalization stage on images of character "A" using $\beta = 800$. Fig. 8 shows one normalized image of each of the lakes.

This scale and translation invariancy stage does affect two of the Zernike features. Those features are $|A_{00}|$ and $|A_{11}|$. $|A_{00}|$ is going to be the same for all images and $|A_{11}|$ is equal to zero. This is

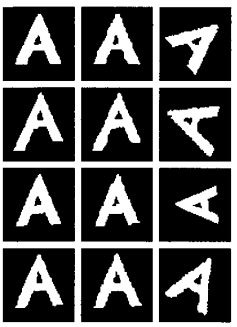

Fig. 7. The scale and translation normalized images of those shown in Fig. 4.

Fig. 8. The scale and translation normalized images of lakes. One out of the twelve images per lake is shown.

seen by noting

$$\begin{aligned} C_{00} &= \frac{2}{\pi} \int \int_{x^2+y^2 \le 1} g(x, y) R_{00}(\rho)\, dx\, dy \\ &= \frac{2}{\pi} \int \int_{x^2+y^2 \le 1} g(x, y)\, dx\, dy = \frac{2}{\pi} m_{00} \end{aligned} \tag{19}$$

and

$$S_{00} = 0. \tag{20}$$

Since $m_{00} = \beta$ it is evident that $|A_{00}| = |(C_{00}/2) - j(S_{00}/2)| = \beta/\pi$ for all the normalized images. Therefore, $|A_{00}|$ is not taken as one of the features utilized in the classification. For $|A_{11}|$,

$$\begin{aligned} C_{11} &= \frac{4}{\pi} \int \int_{x^2+y^2 \le 1} g(x, y) R_{11}(\rho) \cos\theta\, dx\, dy \\ &= \frac{4}{\pi} \int \int_{x^2+y^2 \le 1} g(x, y) \rho \cos\theta\, dx\, dy \\ &= \frac{4}{\pi} \int \int_{x^2+y^2 \le 1} g(x, y) x\, dx\, dy = \frac{4}{\pi} m_{10} \end{aligned} \tag{21}$$

and

$$\begin{aligned} S_{11} &= \frac{4}{\pi} \int \int_{x^2+y^2 \le 1} g(x, y) R_{11}(\rho) \sin\theta\, dx\, dy \\ &= \frac{4}{\pi} \int \int_{x^2+y^2 \le 1} g(x, y) \rho \sin\theta\, dx\, dy \\ &= \frac{4}{\pi} \int \int_{x^2+y^2 \le 1} g(x, y) y\, dx\, dy = \frac{4}{\pi} m_{01}, \end{aligned} \tag{22}$$

since $m_{10} = m_{01} = 0$ for all normalized images, then $|A_{11}| = |(C_{11}/2) - j(S_{11}/2)| = 0$ for them, and $|A_{11}|$ will not be included as one of the utilized feature. Thus in the following experiments, the extracted Zernike features start from the second order moments.

C. Classification Rules

Two different classifiers namely nearest-neighbor (NN) and minimum-mean-distance (MMD) are used in this study. The description of each follows.

The nearest-neighbor classifier labels an unknown image represented by an m-dimensional feature vector $\boldsymbol{X} = [x_1, x_2, \cdots, x_m]$ with the label of the nearest neighbor of $\boldsymbol{X}$ among all the training

samples. The distance between $\boldsymbol{X}$ and a training sample is measured using Euclidean distance. This is a mapping from m-dimensional feature space onto a one-dimensional Euclidean space. However, to prevent the domination of a subgroup of features, one has to normalize the features. The normalization consists of subtracting sample mean and dividing by standard deviation of the corresponding class.

In a c class problem let $\boldsymbol{t}_k^{(i)} = [t_{k1}^{(i)}, t_{k2}^{(i)}, \cdots, t_{km}^{(i)}]$ and N_i denote the kth m-dimensional training feature vector of the ith class and the number of available training samples of class i, respectively. The unknown test sample $\boldsymbol{X}$ is classified to class i^*, where

$$i^* = \min_i d(\boldsymbol{X}, \boldsymbol{t}_k^{(i)}) \qquad i = 1, 2, \cdots, c$$
$$k = 1, 2, \cdots, N_i \tag{23}$$
$$d(\boldsymbol{X}, \boldsymbol{t}_k^{(i)}) = \left[\sum_{j=1}^{m} (\hat{x}_j - \hat{t}_{kj}^{(i)})^2 \right]^{1/2}$$
$$\hat{x}_j = \frac{x_j - \bar{t}_j^{(i)}}{\sigma_{t_j}^{(i)}}, \quad \hat{t}_{kj}^{(i)} = \frac{t_{kj}^{(i)} - \bar{t}_j^{(i)}}{\sigma_{t_j}^{(i)}}$$

with $\bar{t}_j^{(i)}$ and $\sigma_{t_j}^{(i)}$ representing the sample mean and standard deviation of the jth element of the m-dimensional training feature vector of class i.

The second classifier is a weighted minimum-mean-distance rule. Each class is represented by the sample means and variances of its training features. The utilized classifier measures the sum of the squared distance between the feature vector of the test image $\boldsymbol{X}$ and the mean of the feature vectors of each of the classes weighted by the inverse of the corresponding variances. The purpose of weighting is to balance the effect of each of the m components of the feature vector.

Let $d(\boldsymbol{X}, i)$ be the weighted distance between test image $\boldsymbol{X}$ and representation of class i. Then

$$d(\boldsymbol{X}, i) = \sum_{j=1}^{m} \frac{(x_j - \bar{t}_j^{(i)})^2}{\sigma_{t_j}^{2(i)}}. \tag{24}$$

$\boldsymbol{X}$ is classified to class i^* for which the distance $d(\boldsymbol{t}, i)$ is minimum among $\{d(\boldsymbol{X}, i)\ i = 1, 2, \cdots, c\}$.

D. Error Estimation Schemes

To estimate the error rate associated with the selected features, the available samples must be divided into two sets, one for training (design) and one for testing. Three different partitioning schemes are considered. The first method is known as "leave-one-out." This means that out of N samples from c classes per database, $N - 1$ of them are used to train the classifier and the remaining one to test it. This process is repeated N times, each time leaving a different sample out. Therefore, all of samples are ultimately used for testing. The ratio of the number of misclassifications to the total number of tested samples yields an upper bound of the classification error for the considered set [4]. Since the number of samples in the lake data set is rather small, it is only tested with this scheme. But, for the character data set two additional partitionings are considered.

In a leave-one-out scheme the classifier is trained on rotated images. To test the rotation invariance power of the features, a second partitioning method is considered. In this scheme called "trained on unrotated," the classifier is trained on the four unrotated images per character and tested using the remaining rotated images. This translates into 104 training and 208 test samples.

In the above two cases the classifier sees all four silhouettes of each character during the training phase. The third partitioning scheme is designed to test the sensitivity of the method to slight variations in shape. The classifier is trained on three images of only one of the four silhouettes per character and is tested using the remaining nine images from the other three silhouettes. This means 78 training and 234 test samples are considered. This method is refered to as "train on one silhouette."

E. Classification Results

To decide on n^*, eight images per class are used. In the case of character data set, two images from each of the four silhouettes per character are used. The selected threshold is $\epsilon = 300$ pixels. The rationale for selection of this number is that it represents around 10% difference between the original and the reconstructed image which is a good degree of closeness. The relation between ϵ and n^* is shown later in this section. Tables IV and V list the obtained n^* along with the Hamming distance of $H(\hat{f}_{n^*}, f)$ for each of the eight considered images in the two data sets. A slight modification to the algorithm was allowed which limits the maximum order to 12. Therefore, for some of the eight images of three characters, B, P, and R which do not satisfy the closeness criterion for $n \leq 12$, $n^* = 12$ is selected and no higher order is considered. Based on these results, it is concluded that for the character data set, one needs to extract up to twelfth order Zernike moments corresponding to 47 features. For the lake data set, up to eighth order moments corresponding to 23 features are sufficient. The features are not weighted. The effect of weighting is investigated later.

The classification accuracy rates obtained for the character data set using 47 features and the three described error estimation schemes are listed in the first row of Table VI. In the same table classification results using orders lower than 12 are also presented. Table VII provides a relationship between ϵ and the selected order.

For the lake data set only leave-one-out method along with the minimum-mean-distance classifier is considered. A perfect classification accuracy is obtained.

F. Effect of Feature Weighting

In the next set of experiments, the utilized features are weighted according to the scheme described earlier. The resulting recognition accuracies are very close to those obtained using the unweighted features. In each case either no improvement is observed or at most the error is decreased by one sample. This is expected since for the considered data sets, the unweighted results are very accurate to start with, leaving very little room for improvement. However, it can be argued that the absence of any performance degradation validates the proposed feature weighting scheme.

G. Effect of Missing Phase Information

The considered features are the magnitudes of complex Zernike moments. The phase information is dropped to obtain rotation invariance. The effect of deletion of phase information on classification is investigated through a set of experiments involving four unrotated images of each character. These are the images shown in the first column of Fig. 4 and images presented in Fig. 5. The first two images per character are used for training and the remaining two for testing. The nearest neighbor classifier is utilized. Two sets of experiments are carried out. In the first set, both magnitudes and phases are used as features while in the second set only magnitudes are considered. Perfect recognition accuracies are obtained for both cases when the maximum allowable order is $7 \leq n^* \leq 12$. When $n^* = 6$, magnitudes and phases give perfect accuracy while magnitudes only yield a 98% rate (one error in 52 tests). Thus it can be inferred that the influence of loss of phase information in classification is rather insignificant especially when high order moments are included.

H. Performance Comparisons

In this section, the performance of Zernike features is compared to those of moment invariants and regular moments. In the case of moment invariants six features are utilized since generating a bigger number of them is not a trivial task. These features are $\log_{10} |\phi_i|$, $i = 1, 2, \cdots, 6$ where the ϕ_i's are defined in [7]. Note that in this case there is no need to normalize the images since the ϕ_i's are not only invariant to rotation but also to scale and translation. The same classifiers and error estimation schemes are utilized and the results are listed in the third row of Table VIII. We also ex-

TABLE IV
n^*'S AND $H(\hat{f}_{n^*}, f)$'S FOR EIGHT PROTOTYPE IMAGES OF CHARACTER DATA SET. THE LAST COLUMN SHOWS THE SELECTED n^* (MAXIMUM n^* AMONG EIGHT) FOR EACH CLASS

	1	2	3	4	5	6	7	8	
	n^*,H	n^*,H	n^*,H	n^*,H	n^*,H	n^*,H	n^*,H	n^*,H	n^*
A	7,225	10,285	7,25	7,285	7,219	10,264	7,216	10,248	10
B	12,375	12,429	12,242	12,371	12,372	12,431	12,237	12,377	12
C	9,194	9,209	9,245	9,230	9,203	9,281	9,214	9,255	9
D	11,273	12,288	11,259	12,225	10,221	12,302	12,286	12,231	12
E	10,230	12,270	9,278	12,298	11,262	12,302	9,291	12,299	12
F	11,272	10,268	11,237	11,240	11,222	10,215	11,253	11,241	11
G	9,272	11,256	12,243	10,294	9,296	9,292	12,284	10,287	12
H	10,146	10,180	10,184	12,287	10,220	10,145	10,165	11,295	12
I	6,231	8,104	8,144	8,106	6,294	8,156	8,140	8,123	8
J	8,263	8,288	9,199	9,217	9,134	8,294	9,225	9,207	9
K	11,245	11,259	9,248	11,261	10,282	11,287	9,258	9,297	11
L	8,259	9,203	9,243	8,289	8,236	8,262	9,251	8,284	9
M	9,267	11,272	11,272	9,288	9,280	11,279	11,287	10,279	11
N	8,214	8,298	8,290	11,207	8,224	8,299	8,273	11,191	11
O	12,150	12,220	12,226	12,207	12,191	12,160	12,205	12,220	12
P	12,365	12,389	12,345	12,249	12,303	12,339	12,326	12,224	12
Q	12,316	11,247	12,297	12,311	12,284	11,272	12,289	12,255	12
R	10,245	12,385	12,443	12,437	10,248	12,410	12,476	12,327	12
S	10,227	11,271	12,185	11,149	11,146	11,230	11,289	12,255	12
T	9,291	8,280	9,296	9,286	8,290	9,202	10,141	9,295	10
U	10,164	8,240	10,170	9,290	10,147	8,253	10,139	10,185	10
V	7,253	10,174	10,208	10,175	9,277	10,176	10,213	10,185	10
W	11,280	11,261	12,266	12,219	12,198	11,225	12,246	11,250	12
X	12,253	12,272	12,266	12,253	12,240	12,247	12,237	12,281	12
Y	9,259	9,225	10,239	11,247	10,217	9,208	10,270	11,291	11
Z	12,287	12,137	12,258	12,270	12,163	12,142	12,237	12,268	12

TABLE V
n^*'S AND $H(\hat{f}_{n^*}, f)$'S FOR EIGHT PROTOTYPE IMAGES OF LAKE DATA SET. THE LAST COLUMN SHOWS THE SELECTED n^* (MAXIMUM n^* AMONG EIGHT) FOR EACH CLASS

	1	2	3	4	5	6	7	8	
	n^*,H	n^*,H	n^*,H	n^*,H	n^*,H	n^*,H	n^*,H	n^*,H	n^*
ERI	8,124	8,135	8,125	6,295	8,124	8,147	8,125	8,134	8
HRN	7,229	7,212	7,233	7,218	7,225	7,240	7,228	5,297	7
MCH	8,152	8,157	8,157	8,162	8,180	8,160	8,154	6,286	8
SPR	5,234	5,229	5,204	5,229	5,233	5,226	5,209	5,229	5

perimented with such features extracted from translation and scaled normalized images and got very similar classification results.

Unlike moment invariants, regular moments m_{pq} could be constructed for any positive p and q. However, as noted earlier, they are not rotation invariant. To experiment with them, the images need to be corrected for rotation as well. This is done by the method of principal axis described in [15]. After translation and scale normalization, the principal axis of the image is found and it is rotated such that this axis lines up with the horizontal axis. However, there are problems associated with this technique. If the image is n-fold symmetric, there will be multiple possible sets of principal axes. In the case of a character data set, such a problem happened for some of the symmetric characters like "C". In addition, the presence of even a moderate amount of noise significantly affects the accuracy of rotation correction.

To do a fair comparison, 47 regular moments are extracted from translation, scale, and rotation normalized images. The pq orders are the same as mn orders of the considered Zernike moments. The same classifiers and error estimation schemes are utilized and the results are presented in the second row of Table VIII.

The entries of Table VIII clearly verify the assertion regarding superiority of Zernike moment features over moment invariants and regular moments. The same relative strength is preserved if less than twelfth orders are considered.

I. Performance on Noisy Images

In this section, the noise tolerance and sensitivity of the Zernike features are studied experimentally. Eight noisy images with different orientations are generated for each character by randomly selecting some of the 4096 pixels of a normalized noise-free binary image and reversing their values from 0 to 1 or vice versa. The random pixel selection is done according to a uniform distribution between 1 and 4096. Different sets with different noise levels are generated. The signal-to-noise ratio (SNR) of the generated sets are 30 dB, 25 dB, and 17 dB. Fig. 9 shows one of the eight noisy images of characters "A" and "B" for different SNR's. Although the square images are shown, only the unit circle portion of them are used in the experiments. Using the noise-free normalized images as training samples, and the noisy images as test samples, the performance of the features are tested in three sets of experiments. All twelve clean translation and scale normalized images, only the four unrotated images, and only the three from one silhouette image are used for training in the first, second, and third sets of experiments, respectively. The results are tabulated in Tables IX, X, and XI. In [17] it is shown that higher order moments are more sensitive to noise. Our experiments verify this point since including them in many cases degrades the accuracy. Overall, the performance is rather good when SNR is 25 dB or higher.

TABLE VI
RECOGNITION ACCURACY RATES FOR THE CHARACTER DATA SET USING ZERNIKE FEATURES. NN AND MMD STAND FOR NEAREST-NEIGHBOR AND MINIMUM-MEAN-DISTANCE CLASSIFIERS, RESPECTIVELY

Maximum Order	Leave one out		Train on unrotated		Train on one silhouette	
	NN	MMD	NN	MMD	NN	MMD
12 (47 features)	99	97	95	93	93	90
11 (40 features)	99	96	95	92	92	90
10 (34 features)	98	95	94	91	92	90
9 (28 features)	97	95	92	91	90	89
8 (23 features)	97	95	91	90	89	86

TABLE VII
THE RELATION BETWEEN THRESHOLD ϵ (IN PIXELS) AND THE SELECTED MAXIMUM ORDER

ϵ	n*
300	12
350	11
410	10
470	9
560	8

TABLE VIII
PERFORMANCE COMPARISONS AMONG ZERNIKE, REGULAR MOMENTS, AND MOMENT INVARIANT FEATURES

Feature Type	Leave one out		Train on unrotated		Train on one silhouette	
	NN	MMD	NN	MMD	NN	MMD
Zernike Features (47)	99	97	95	93	93	90
Regular Moments (47)	90	82	86	76	81	71
Moment Invariants (6)	76	54	66	45	58	40

VII. CONCLUSION

In this correspondence, a new set of features defined on the Zernike moments which are a mapping of an image function onto a set

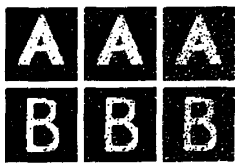

Fig. 9. One out of the eight noisy images of characters A and B. From left to right SNR is 30 dB, 25 dB, and 17 dB.

TABLE IX
RECOGNITION ACCURACY RATES FOR THE NOISY CHARACTER DATA SET. THE CLASSIFIERS ARE TRAINED ON ALL TWELVE CLEAN IMAGES PER CHARACTER

Maximum Order	30 dB		25 dB		17 dB	
	NN	MMD	NN	MMD	NN	MMD
12	92	87	87	85	62	57
11	92	85	86	84	60	56
10	90	86	83	83	65	59
9	91	88	85	86	69	62
8	91	92	89	88	68	62
7	90	93	90	88	62	57
6	89	91	88	87	60	52

TABLE X
RECOGNITION ACCURACY RATES FOR THE NOISY CHARACTER DATA SET. THE CLASSIFIERS ARE TRAINED ON FOUR UNROTATED CLEAN IMAGES PER CHARACTER

Maximum Order	30 dB		25 dB		17 dB	
	NN	MMD	NN	MMD	NN	MMD
12	86	84	85	82	57	53
11	86	80	83	80	55	50
10	84	81	81	80	54	53
9	83	80	82	81	56	52
8	85	84	86	82	59	54
7	86	83	86	83	58	53
6	85	81	85	82	57	52

of orthogonal basis functions over the unit circle has been developed. These features are the magnitudes of complex Zernike moments and are proven to be rotation invariant. The orthogonality property of Zernike moments makes the image reconstruction from its moments computationally simple. Moreover, it enables one to evaluate the image representation ability of each order moment as well as its contribution to the reconstruction process. Based on this property a systematic method for selection of the required number of features in a classification problem is developed. The selected number for the highest order moment is the one which yields a reconstructed image which is close to the original one. The discrimination power of the proposed Zernike moment features and the developed feature selection method are tested by a series of experiments on two different data sets using a nearest-neighbor as well as a minimum-mean-distance classifier. The considered images have differences in scale, translation, and rotation. They are first normalized with respect to scale and translation using regular moment based techniques. The obtained classification accuracy for a 26-class character data set is 99%, while a perfect recognition rate is reported for 4-class lake data set. Thus one can conclude that the proposed features and the accompanying feature selection method are quite effective for the image classification problem. In addition the superiority of Zernike moment features over regular moments and moment invariants is shown. Finally, the noise sensitivity of Zernike features is studied and it is concluded that they can perform well in the presence of a moderate level of noise.

TABLE XI
RECOGNITION ACCURACY RATES FOR THE NOISY CHARACTER DATA SET. THE CLASSIFIERS ARE TRAINED ON THREE IMAGES OF ONE OF THE SILHOUETTES PER CHARACTER

Maximum Order	30 dB		25 dB		17 dB	
	NN	MMD	NN	MMD	NN	MMD
12	83	81	82	78	50	47
11	82	79	80	76	49	45
10	82	79	79	77	52	48
9	79	81	81	78	52	48
8	81	82	83	81	54	50
7	81	81	84	80	53	48
6	78	79	83	80	54	48

REFERENCES

[1] Y. S. Abu-Mostafa and D. Psaltis, "Image normalization by complex moments," *IEEE Trans. Pattern Anal. Machine Intell.*, vol. PAMI-7, no. 1, pp. 46-55, Jan. 1985.

[2] S. A. Dudani, K. J. Breeding, and R. B. McGhee, "Aircraft identification by moment invariants," *IEEE Trans. Comput.*, vol. C-26, no. 1, pp. 39-45, Jan. 1983.

[3] K. S. Fu, *Syntactic Pattern Recognition and Application.* Englewood Cliffs, NJ: Prentice-Hall, 1982.

[4] K. Fukunaga, *Introduction to Statistical Pattern Recognition.* New York: Academic, 1972.

[5] R. C. Gonzalez and P. Wintz, *Digital Image Processing.* Reading, MA: Addison-Wesley, 1977.

[6] Y. N. Hsu, H. H. Arsenault, and G. April, "Rotational invariant digital pattern recognition using circular harmonic expansion," *Appl. Opt.*, vol. 21, pp. 4012-4015, 1982.

[7] M. K. Hu, "Visual pattern recognition by moment invariants," *IRE Trans. Inform. Theory*, vol. IT-8, pp. 179-187, Feb. 1962.

[8] R. E. Johnson, F. L. Kiokemeister, and E. S. Wolk, *Calculus with Analytic Geometry*, 6th ed. Boston, MA: Allyn and Bacon, 1978.

[9] R. L. Kashyap and R. Chellappa, "Stochastic models for closed boundary analysis: Representation and reconstruction," *IEEE Trans. Inform. Theory*, vol. IT-27, pp. 627-637, Sept. 1981.

[10] A. Khotanzad and Y. H. Hong, "Rotation and scale invariant features for texture classification," in *Proc. Robotics and Automation, IASTED*, Santa Barbara, CA, May 1987, pp. 16-17.

[11] ——, "Rotation invariant pattern recognition using Zernike moments," in *Proc. 9th ICPR*, Rome, Italy, Nov. 1988, pp. 326-328.

[12] A. Krzyzak, S. Y. Leung, and C. Y. Suen, "Reconstruction of two-dimensional patterns by Fourier descriptors," in *Proc. 9th ICPR*, Rome, Italy, Nov. 1988, pp. 555-558.

[13] S. Maitra, "Moment invariants," *Proc. IEEE*, vol. 67, no. 4, pp. 697-699, Apr. 1979.

[14] E. Persoon and K. S. Fu, "Shape discrimination using Fourier descriptors," *IEEE Trans. Syst., Man, and Cybern.*, vol. SMC-7, pp. 170-179, Mar. 1977.

[15] A. P. Reeves, R. J. Prokop, S. E. Andrews, and F. Kuhl, "Three-dimensional shape analysis using moments and Fourier descriptors," *IEEE Trans. Pattern Anal. Machine Intell.*, vol. 10, no. 6, pp. 937-943, Nov. 1988.

[16] M. Teague, "Image analysis via the general theory of moments," *J. Opt. Soc. Amer.*, vol. 70, no. 8, pp. 920-930, Aug. 1980.

[17] C. H. Teh and R. T. Chin, "On image analysis by the methods of moments," *IEEE Trans. Pattern Anal. Machine Intell.*, vol. 10, no. 4, pp. 496-513, July 1988.

[18] C. T. Zhan and C. T. Roskies, "Fourier descriptors for plane closed curves," *IEEE Trans. Comput.*, vol. C-21, pp. 269-281, Mar. 1972.

[19] F. Zernike, *Physica*, vol. 1, p. 689, 1934.